Vertical axis turbine simulations based on sliding and overset meshes

IOP Conf. Series: Materials Science and Engineering **1312** (2024) 012010 doi:10.1088/1757-899X/1312/1/012010

Vertical axis turbine simulations based on sliding and overset meshes

Asmelash Haftu Amaha[1], Shivasubramanian Gopalakrishnan[1], Prabhu Ramachandran[1] and Joel Guerrero[2]

[1]Indian Institute of Technology Bombay, Powai 400076, Maharashtra, India
[2]Wolf Dynamics, Genoa 16127, Liguria, Italy

E-mail: asmelash.a@aero.iitb.ac.in

Abstract. Vertical Axis Turbines (VATs) are gaining traction as decentralized energy sources due to their simple design and suitability for various wind conditions. However, understanding VAT aerodynamics requires robust computational methods. This study compares the accuracy and efficiency of two meshing techniques (sliding mesh and overset mesh) for VAT simulations using OpenFOAM. Validation against experimental data confirms the capability of both methods to capture flow physics and predict turbine performance. The results suggest both techniques offer efficient and accurate VAT simulations, providing valuable tools for future VAT optimization and experimental validation.

1. Introduction

The horizontal axis wind turbine (HAWT) and vertical axis wind turbine (VAWT or VAT) are the leading devices for harnessing renewable energy from the wind. Currently, HAWTs are more advanced with improvements in size and aerodynamic efficiency, achieving a power coefficient close to the 50% range which is about 85% of the Betz limit [1, 2]. They are, however, very expensive to achieve affordable and distributed modern energy systems and sustainability goals [3]. VATs also called cross-flow turbines were widely studied by Sandia from 1970 to 1990, and a resurgence of interest is seen from 2010 till date. VATs can have one or more straight or curved blades that rotate parallel to the axis of rotation.VATs have some attractive features compared to HAWTs. They are compact, independent of the flow direction, the mass is concentrated near ground level hence low operation and maintenance (OM) costs, and used for a wide range of applications including adaptability for small-scale domestic installations. In addition, VATs can supplement HAWTs or be employed in places where HAWTs are less effective, for example in Class 2 wind sites. Class 2 wind site can be considered as a moderately breezy location (5.4 to 6.4 m/s) that is not quite as windy as Class 3 or above. This

may not be the windiest site around, but they still offer the potential for wind energy development and are major wind sites in many countries of the world [4].

VAT blades experience complex unsteady aerodynamics, largely due to the blade motion inducing pressure differences in the vicinity. These pressure fluctuations interact with the freestream velocity in the upstream region and with the wake in the downstream region of the rotor. This unsteadiness is inherent and persists even if the wind speed is constant or the rotor speed is constant. Due to such complexities, accurate simulation of VAT performance is a challenging task and requires accurate meshing techniques [5, 6, 7, 8] and [9, 10, 11].

Numerous analytical and computational models have been developed in the past to analyze the aerodynamic performance of several VAT designs, ranging from the simple Blade Element Momentum (BEM) model approaches to more advanced CFD simulations. While CFD models are essential for accurate predictions, their reliability relies heavily on factors such as mesh generation technique, turbulence model selection, and appropriate boundary conditions. Among the existing literature, the sliding mesh technique is predominantly utilized for CFD simulations of VATs [2, 12]. However, it is noteworthy that only a limited number of studies have explored alternative techniques to the sliding mesh approach such as the overset mesh [13, 14] and morphing mesh [13, 15].

OpenFOAM is a powerful and flexible open-source computational fluid dynamics (CFD) code platform for simulating fluid flow and related phenomena in computational continuum mechanics [16]. Since its initial release in 2004, OpenFOAM is now a popular open-source CFD platform with a strong community of users and developers, accounting for 39% of all the CFD software usage till 2018 in wind energy conversion systems [17].

The dynamic mesh capability of OpenFOAM enables the simulation of moving objects and changing boundaries, making it a valuable tool for a wide range of CFD simulations involving complex motion scenarios. It provides several dynamic mesh classes such as adaptive mesh refinement (AMR), moving meshes (Whole domain), morphing meshes (Smoothing), sliding meshes (SM), and overset meshes (OM). In this work, we employed both SM and OM techniques for simulating vertical axis turbines.

The motivation and objectives of this study are (1) exploring the complex aerodynamics of vertical axis turbines, and (2) using computational fluid dynamics to analyze these sophisticated systems. It aims to explore vertical-axis turbines and advance computational modeling methods in this area by delving into the intersection of aerodynamics and CFD. In CFD, the sliding mesh technique is an established simulation model for many complex systems. Due to its flexibility to use for more complex geometries, the overset mesh technique is gaining more attention in academia and industries. This inspires us to explore its capability for accurately simulating VATs, which are also the research targets for decentralized and sustainable energy supply. The main focus is to provide a thorough comparison between sliding mesh and overset mesh methods by underlining the differences, advantages, and limitations of each. The comparison focuses on convergence and sensitivity studies, investigation of the flow field parameters, and the analysis of aerodynamic and performance parameters, which can contribute to understanding complex flow phenomena and optimizing simulation approaches.

2. Blade Aerodynamic Forces

The problem chosen for this comparison is the VAT based on Darrieus type H-rotor commonly employed for wind and hydrokinetic applications on small scales. Figure 1 shows the schematic diagram of three commonly used three bladed vertical axis turbines (VATs) used in wind energy. These are (a) H-Darrieus turbine, (b) Darrieus turbine, and (c) Helical-Darrieus turbine. The vertical axis supports the rotor with blades spinning perpendicular to the ground, like a cylinder with wings. The wind pushes or pulls on the blades, causing them to rotate around the vertical axis.

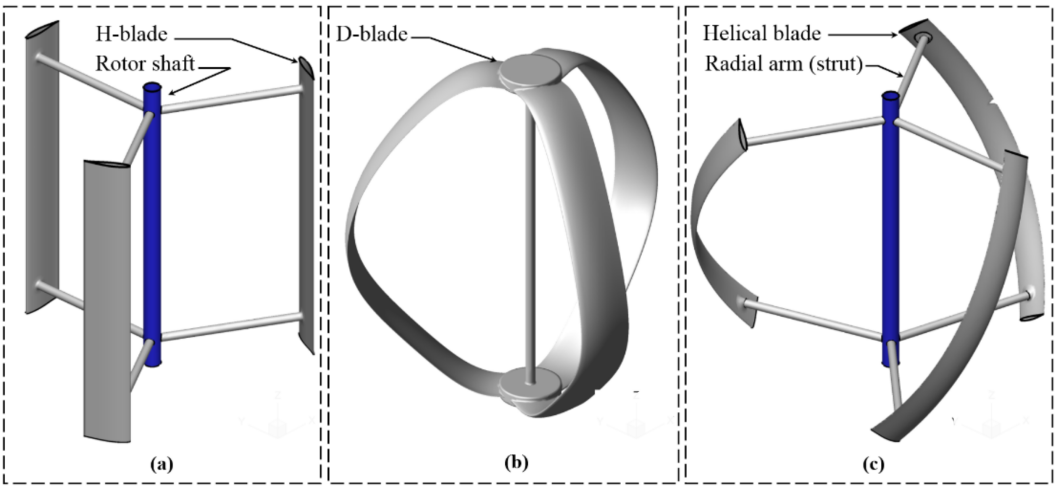

Figure 1: Schematic diagram of vertical axis turbines (VATs) used in wind energy. (a) H-Darrieus turbine, (b) Darrieus turbine, and (c) Helical-Darrieus turbine [18].

The aerodynamic efficiency of a vertical axis wind turbine (VAT) is expressed by the variation of the power coefficient curve, C_p, with a dimensionless tip speed ratio (TSR or λ). It is the ratio of extracted power to the available power. TSR and solidity (σ) are other commonly used dimensionless parameters to describe the performance and operation of a VAT blade are

$$C_p = \frac{P}{\frac{1}{2}\rho U_0^3 A_s}, \quad \lambda = \frac{\omega R}{U_0}, \quad \sigma = \frac{Nc}{R}, \tag{1}$$

where ρ is the density, U_0 is the free stream velocity, $A_s = DH = 2RH$ is area swept by the rotating blade, R is radius of the turbine ($D/2$), H is the height, P is power extracted by the turbine, ω is the angular velocity in rad/s, c is the chord length, and N the number of blades.

The Reynolds number (Re) is also obtained using the chord length and the blade tip speed. It can be defined as

$$Re = \frac{U_t c}{\nu}, \quad U_t = \omega R = U_0 \lambda, \tag{2}$$

where ν is the kinematic viscosity of the fluid and U_t is blade tip speed.

Figure 2 illustrates the schematic diagram of the top view of a single turbine rotor along its flight path, which is H-type Darrieus VAT with symmetric NACA blades. The upwind and downwind regions as well as the different flow segments are discussed in a later section. Figure 3 shows the aerodynamic forces acting on the VAT rotating in the counterclockwise direction. For, a multi-blade turbine, the rotor blades, each of height H, are initially evenly spaced at a radial distance R around the central axis, which is the vertical shaft. Throughout the rotation of the turbine (see Figure 3), airflow dynamics

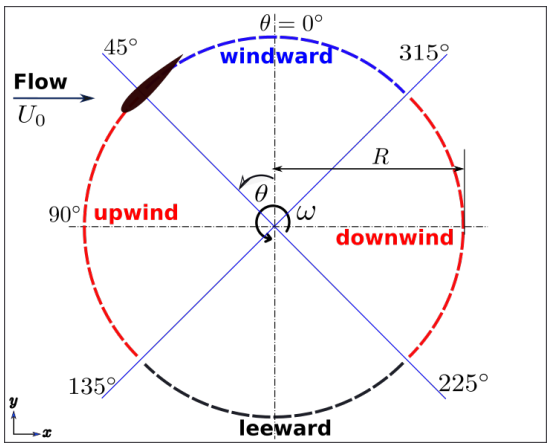

Figure 2: Schematic diagram for a VAT simulation and the computational domain with fixed and static components and boundary conditions.

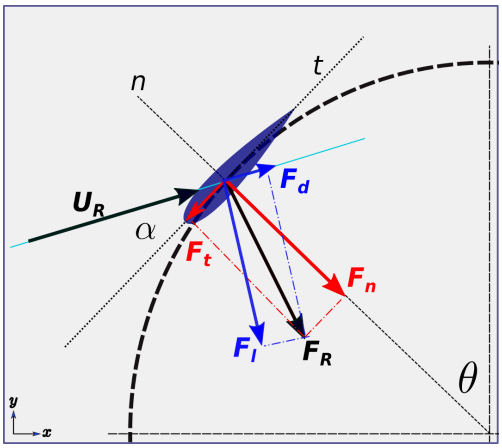

Figure 3: Schematic diagram and aerodynamic forces at a specific azimuth angle of VAT. Blade motion starts from $\theta = 0°$.

around the blades generate reaction forces, such as the lift F_l, drag F_d, normal force F_n and tangential forces F_t. The force, F_R is the resultant of the forces and U_r is the relative velocity. The dimensionless normal and tangential coefficients of these forces are revised as shown,

$$\begin{cases} C_n &= F_n/(0.5\rho U_0^2 A_b), \\ C_t &= F_t/(0.5\rho U_0^2 A_b), \end{cases} \tag{3}$$

where F_n and F_t are the normal and tangential forces of the blade flight path, and C_n and C_t are the coefficients, and F_l and F_d are obtained as a function the relative velocity and angle of attack.

3. Computational method

3.1. Governing Equations

Cells of small volumes form a mesh to describe the solution domain and in CFD simulations and in many cases the mesh remains stationary. In the case of a dynamic mesh, the mesh changes based on the motion of the solution domain or it changes topologically, this feature also works when a domain is decomposed for parallel simulation.

Utilizing the finite volume method (FVM), OpenFOAM solves the Reynolds transport theorem (RTT) in the integral form (as depicted in equation 4) [19, 20, 21, 22]. It represents the general transport equation for the flow property ϕ.

$$\int_{V_p} \frac{\partial \rho\phi}{\partial t} \mathrm{dV} + \int_{V_p} \nabla \cdot [\rho\phi(\mathbf{u} - \mathbf{u}_g)] dV - \int_{V_p} \nabla \cdot (\rho\Gamma_\phi \nabla\phi) dV = \int_{V_p} S_\phi \phi dV, \tag{4}$$

where $\mathbf{u}$, p, and ρ are the flow velocity, the fluid pressure, and density, respectively. $\mathbf{u}_g$ is the mesh velocity in dynamic meshes which modifies the convective part of the equation, and the volume dV is a function of time indicating that shape of the cells is changing in time.

By considering the assumptions for incompressible unsteady Navier-Stokes equations (NSE) and accounting for a time-varying computational domain with a moving mesh, equation 4 can be cast into the continuity and momentum equations, as expressed in equations 5 and 6.

$$\nabla \cdot \mathbf{u} = 0 \tag{5}$$

$$\frac{\partial \mathbf{u}}{\partial t} + [(\mathbf{u} - \mathbf{u}_g) \cdot \nabla]\mathbf{u} = -\nabla p/\rho + \nu \nabla^2 \mathbf{u} \tag{6}$$

The sliding mesh and overset mesh techniques are methods for handling cases with dynamic mesh [19, 23]. The two distinct dynamic mesh techniques can be used to simulate VATs and both are briefly introduced in this section. They are convenient and able to simulate the movement of the VAT blades traversing a circular trajectory. The sliding mesh is first applied for the simulation (and validation) of the baseline VAT case. Both methods are discussed along with the CFD model of the turbine and configuration parameters shown in Table 1.

3.2. VAT Configuration and CFD Model

The Darrieus vertical axis turbine (VAT) is numerically investigated in 2D employing the experimental conditions of reference [24]. The simulation involves a single blade with a NACA0015 airfoil, 1.22 m diameter, and a rotational speed of 0.75 rad/sec. These parameters correspond to a Reynolds number of 67,000 and a tip speed ratio of 2.5, with an undisturbed water velocity of 0.183 m/sec. The rotor solidity, defined as the ratio of the airfoil chord to rotor radius, is 0.25, with a chord length of 0.1524 m. Vertical axis turbine with only one blade is not common in the industry, however, it is justifiable to use for research because it makes it more convenient to analyze the flow past its rotor, the aerodynamic blade loads, and the wake characteristics. The inclusion of additional blades is straightforward afterwards. In addition, reference data for validation is available in reference [24]. The parameters of the CFD model and those of the Oler experiment are summarized in Table 1.

3.3. Computational Domain and Boundary Conditions

The 2D computational domain represents a virtual wind tunnel with fixed and rotating components. An AMI interface facilitates mesh motion for the Sliding Mesh (SM) case (Figure 4). In contrast, the Overset Mesh (OM) case (Figure 5) only rotates a portion of the airfoil, eliminating the need for a full rotating core. Both methods utilize blades

Table 1: Parameters for VAT CFD Model

Parameters	**Value**	**Parameters**	**Value**
Airfoil	NACA0015	Reynolds number	67,000
Number of blade, N	1	Tip speed ratio, λ	2.5, 5.1, 7.5
Chord length, c	0.1524 m	Freestream velocity	0.183 m/s
Diameter turbine, D_t	1.22 m	Rotational speed, ω	0.75 rad/s
Diameter of Rotor, D_c	1.5 m	Blade Aspect Ratio	6.5617

(NACA profile) created using python, and the rotor STL (Stereolithography) is generated using Onshape ([25]). The blades act as obstacles within the domain and can perform various motions depending on the case, including rotating for Vertical Axis Turbines (VAT) or flapping for airfoils. The rectangular domain has defined inlet and outlet boundaries on the left and right faces, respectively, while the top and bottom represent the virtual wind tunnel walls.

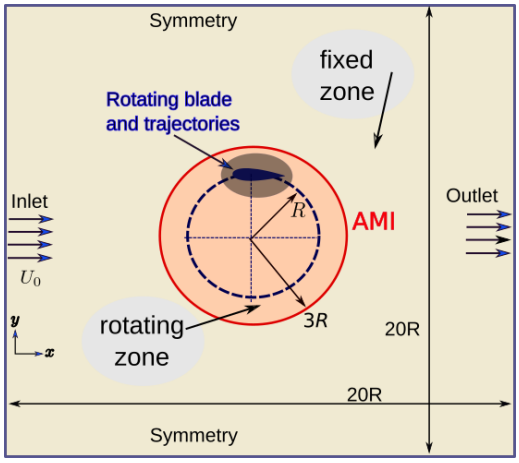

Figure 4: Schematic diagram, computational domain, and boundary conditions of a VAT simulation. Fixed and static components with sliding mesh, AMI.

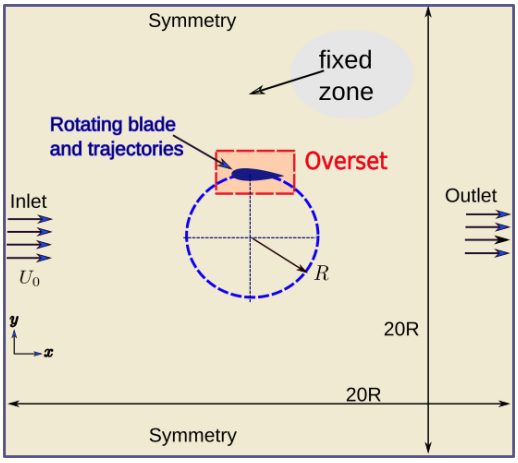

Figure 5: Schematic diagram, computational domain, and boundary conditions of a VAT simulation. Fixed and static components with overset mesh, overset.

The inlet boundary employs a Dirichlet (fixed value) condition for velocity and a Neumann (zero-gradient) condition for pressure. Conversely, the outlet utilizes a Dirichlet condition for pressure and a Neumann condition for velocity. Top and bottom boundaries are treated with symmetry conditions, which mathematically translates to zero normal gradient of velocity (U). For stationary walls, a no-slip boundary condition is enforced. For moving walls like the Vertical Axis Turbine (VAT) surface, a moving wall velocity boundary condition is applied. Finally, the Arbitrary Mesh Interface (`AMI`) technique facilitates data interpolation across the interface boundaries between stationary and moving mesh regions. This technique utilizes a cyclic approach

(`cyclicAMI`) for these interfaces. A detailed summary of the boundary conditions is provided in Table 2.

Table 2: Parameters of the boundary conditions.

Boundary	**Condition**	**Value**
Inlet	Velocity Inlet	$U_0 = 0.183$ m/s, and turbulence
Outlet	Pressure Outlet	$P = 0$ Pa
TopAndBottom	zeroGradient	extrapolated
FrontAndBack	empty	empty
Blade	movingWallVelocity	kqRWallFunction, nutkWallFunction, epsilonWallFunction, omegaWallFunction
Overset	overset	interpolated

3.4. Mesh generation

Two types of meshes are created for the simulations: one for the sliding mesh and another for the overset mesh. In both instances, the mesh exhibits finer resolution near the center and coarser resolution towards the outer region. The coarser mesh is constructed in the background, comprising structured rectangular cells, and refined through various refinement zones. Figure 6 and Figure 7 demonstrate these procedures for SM and OM, respectively.

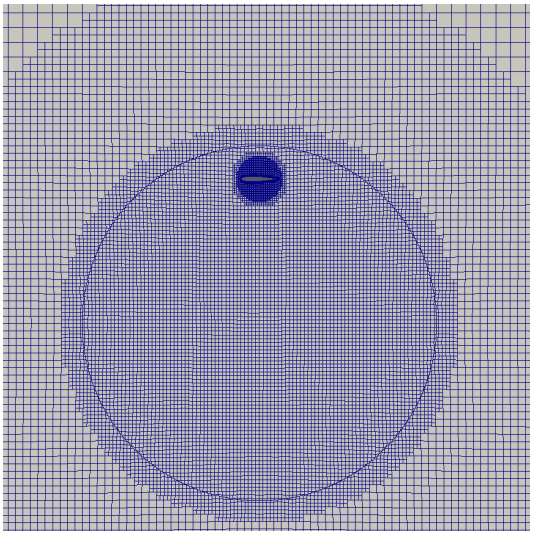

Figure 6: Mesh Generation using SM with AMI.

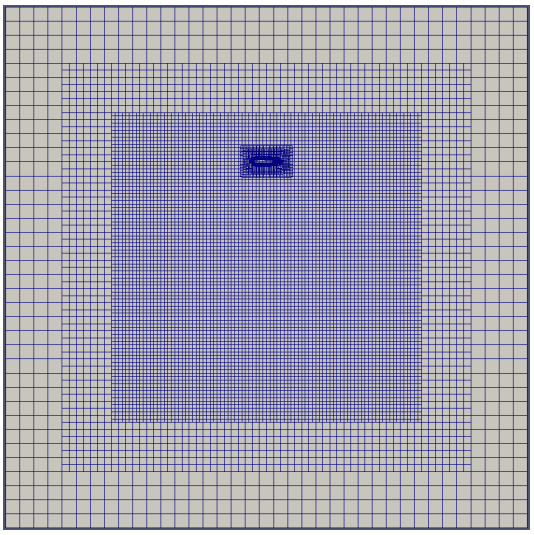

Figure 7: Mesh Generation using OM with overset.

The mesh is constructed using computational tools provided by OpenFOAM, an open-source computational fluid dynamics software package. We adhere to established

guidelines for assessing mesh quality, given the absence of a universally accepted metric. Mesh refinement is determined through grid independence tests, ensuring computational results are not unduly influenced by mesh resolution. Additionally, we evaluate key mesh quality parameters such as orthogonality, skewness, aspect ratio, and smoothness, as recommended in prior studies [26]. Refinement near the airfoil's trailing edge is achieved using specialized settings within the `snappyHexMesh` utility, a feature within OpenFOAM, Table 3. The non-dimensional wall distance, denoted as y^+, is utilized to precisely position the first grid cell adjacent to the airfoil surface. This turbulence parameter is defined as,

$$y^+ = \frac{U_f \times y_\perp}{\nu}, \tag{7}$$

where y^+, U_f, $y_\perp$, and ν are the non-dimensional wall distance, friction velocity, the first cell center distance, and the fluid kinematic viscosity, respectively. The friction velocity is obtained using $U_f = \sqrt{\tau_w/\rho}$. Here, $\tau_w = 0.5\rho {U_0}^2 C_f$ is the wall shear stress and C_f local skin friction coefficient [27]. With wall functions, we can use higher values of $y^+ \sim (10 - 30)$ [28].

The fluctuation of y^+ is driven by the continuous rotation of the VAT blade, leading to alterations in the blade's relative velocity. Notably, the area with the highest relative velocity, typically situated close to the azimuth position of 0 degrees, exerts a significant influence on y^+.

Table 3: Main snappyHexMesh parameters and mesh statistics.

snappyHexMesh parameters	**Values**	**Mesh statistics**	**Values**
resolveFeatureAngle	15	Layers	10
nSolveIter	100	Expansion ratio	1.25
finalLayerThickness	0.7	Total cells	60,446
minThickness	1.16×10^{-4}	Rotor cells	31,320
maxNonOrtho	180	Background cells	29,126
maxBoundarySkewness	-1 (disabled)	Max aspect ratio	4.3576, (OK)
maxInternalSkewness	-1 (disabled)	Max skewness	1.4490, (OK)

Figure 8 show the mesh generation with a successively enlarged view near the airfoil. we first studied the convergence of the tangential force coefficient for the solution sensitivity to gird size, number of revolutions, and time step. The grid that improved the overall accuracy is considered for all simulations, 60,000 cells in this case. The computational domain and boundary conditions are shown in Figure 4.

3.5. Mesh generation: Overset mesh

The traditional moving mesh techniques (sliding meshes, morphing meshes, etc) can simulate moderately challenging problems. However, problems involving complex motions such as those that can be described using `6DOF` or with prescribed motion tables are impossible to simulate using these methods. The Overset Meshes OM or (overlapping grids) is a mesh generation strategy that allows a set of cells (control

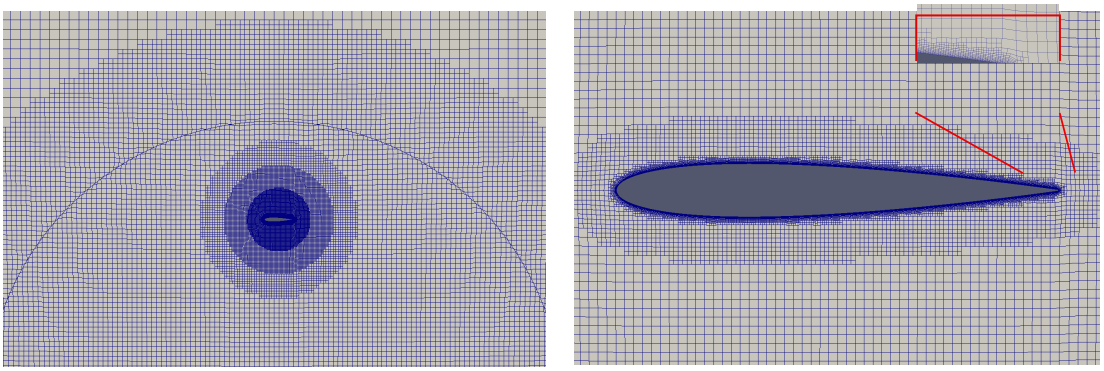

Figure 8: Mesh generation around the airfoil (SM), min edge length of 0.00025 and 10 layers with ER of 1.15. (a) enlarged view close to the airfoil, (b) enlarged view around the airfoil surface.

volumes) to overlap with other sets of grids. OM method enables the simulation of problems that are extremely difficult for traditional moving mesh methods. OM is recognized as an attractive approach for treating complex geometries, single or multiple bodies performing complex movements, allowing great flexibility in modeling them. It is only recently supported by the ESI version of the major open-source software package, OpenFOAM [19, 14, 27].

3.6. Turbulence model specification

Unsteady Reynolds-Averaged Navier-Stokes (URANS) simulations were employed to predict the performance of a Darrieus wind turbine in incompressible flow. We initially evaluated three turbulence models: laminar, SST $k-\omega$, and RNG $k-\epsilon$. The laminar model exhibited oscillatory behaviour and overestimated blade loads, rendering it unsuitable for this application. Conversely, both SST $k-\omega$ and RNG $k-\epsilon$ models produced closely matching and accurate results for the tangential aerodynamic forces. The values for turbulent kinetic energy (k), dissipation rate (ϵ), and specific dissipation rate (ω) are estimated using Eq. 8. We set a 5% turbulent intensity (I) and equate the length scale (l) to the chord length (c). The prescribed boundary conditions require specification of the value of U, k, ϵ and ω.

$$k = \frac{3}{2}(UI)^2, \qquad \epsilon = C_\mu^{0.75} \times \frac{k^{1.5}}{l} \qquad \omega = \frac{\epsilon}{k}, \qquad \nu_t = 0.09\frac{k^2}{\epsilon}, \tag{8}$$

The RNG $k-\epsilon$ (`RNGkEpsilon` in OpenFOAM) model is a commonly used turbulence model suitable for high Reynolds number simulations. It does not directly resolve the viscous sublayer near walls. In OpenFOAM, wall modeling with `RNGkEpsilon` is facilitated by the `kqRWallFunction`, which represents turbulence near walls. For Reynolds number around 67000, a y^+ value between 30 to 100 is computationally efficient. However, it's crucial to ensure a sufficiently refined mesh near walls for accurate results. A y^+ value of approximately 8, although more computationally demanding, is

generally acceptable, capturing the boundary layer's logarithmic region while relying on wall functions to handle the viscous sublayer.

The SST $k-\omega$ model is a widely used two-equation turbulence model that blends the $k-\omega$ formulation in the boundary layer with the $k-\epsilon$ behavior in the free stream [29, 30]. This enables accurate prediction of flows with adverse pressure gradients and separation. Unlike the RNG $k-\epsilon$ model, SST $k-\omega$ directly resolves the viscous sublayer near walls, eliminating the need for wall functions. However, it requires a finer mesh resolution near walls compared to RNG $k-\epsilon$ when using wall functions.

The simulations described in this study utilize OpenFOAM-v9 for the sliding mesh (SM) simulations and ESI OpenFOAM-v2112 for the overset mesh (OM) simulations. The solvers employed are `pimpleMFoam` for the sliding mesh and `OverpimpleDyMFoam` for the overset mesh. The PIMPLE solver, integrating the steady-state SIMPLE [31] and transient PISO methods, adopts a pseudo-transient approach. This hybrid algorithm is particularly suitable for turbomachinery-type problems, providing faster simulations compared to fully transient methods, while maintaining higher accuracy than steady-state solvers.

4. Results and discussion

This section presents the results and analysis of 2D numerical simulations conducted to investigate the performance of a VAT utilizing sliding and overset mesh techniques. We use `pimpleMFoam` with out LTS and `OverpimpleDyMFoam` with LTS for SM and OM respectively. LTS is a versatile technique that can be applied to various types of simulations (steady-state and unsteady) to improve computational efficiency and accuracy. Initial sensitivity and convergence analyses were performed using sliding mesh, followed by validation against experimental data. Next, simulations are conducted using the overset mesh and the results are compared. Due to the availability of reference data for validation and its good performance, all the computations employ the symmetric NACA 0015 airfoil.

For the simulations with sliding mesh (SM), we employ a lower `CFL` number (0.9) and this resulted in stability for the complex turbine motion. The SM simulations apply single time step throughout the domain and do not typically utilize local time stepping (LTS). The average value of y^+ is approximately 5, and backward difference is employed for temporal discretization.

For the simulations with overset mesh (OM), we employ a higher `CFL` number (2.0) was chosen to expedite convergence. We also use local time stepping (LTS) which allows different time steps in different regions of the mesh to improve efficiency for complex geometries. Both cases use the RNGkEpsilon turbulence model with `kqRWallFunction`. The average value of y^+ is around 10, and the `Euler` scheme is employed for temporal discretization.

4.1. Aerodynamic Performance

Figure 9a to Figure 9d illustrate the convergence of tangential force coefficient and the solution sensitivity to gird size, number of revolutions, and time step. The grid that improved the overall accuracy is considered for all simulations, about $60,000$ cells in this case. Figure 9b depicts the convergence with revolution cycles for dynamic mesh

method separately, sliding mesh. From the figure, it can be seen that the sliding mesh does not converge well till the 6th cycle for which the overset mesh converges, and all simulations generally converge after ten rotations. Even though the mesh size is more for the overset case, the simulations are faster.

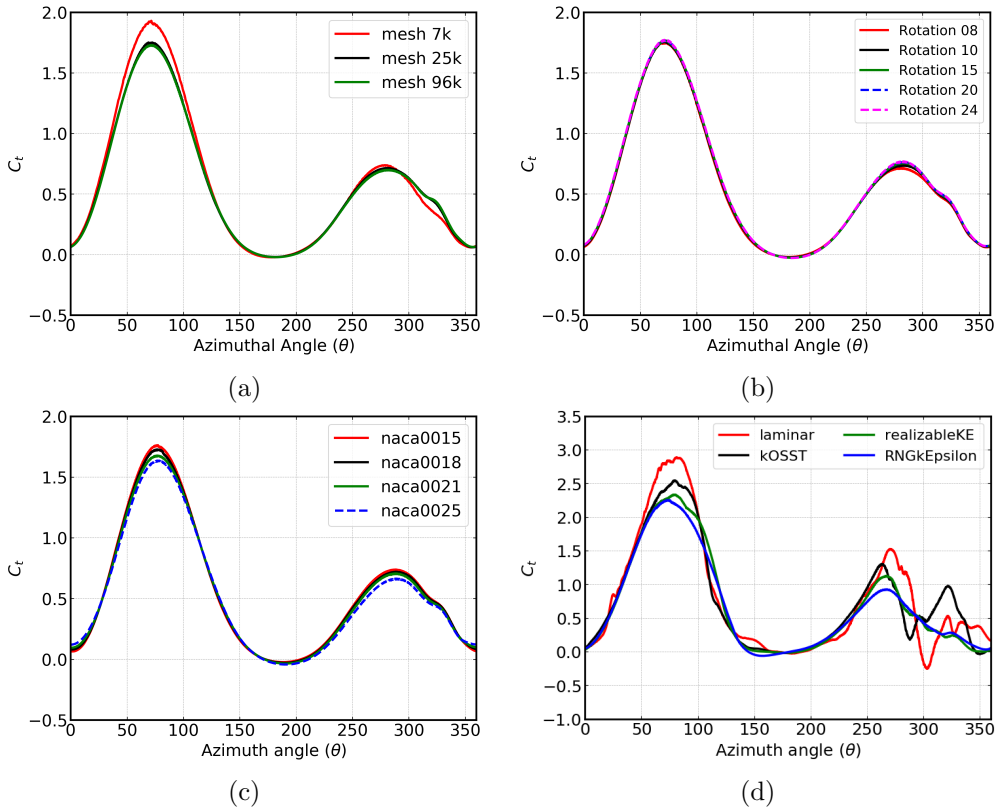

Figure 9: VAT simulation based on SM and sensitivity analysis. (a) mesh sizes, and (b) number of revolutions, (c) blade profiles, and (d) major turbulence models.

Previous studies on VATs have relied on 4-digit symmetric NACA series airfoils, such as NACA0012 [32]. Recent research efforts, however, have ventured into airfoils with higher thicknesses such as the NACA0015, NACA0018, and NACA0021 [32, 33] which offer favourable structural properties, regardless of the associated increase in profile drag. For a comprehensive comparison of their performances, a baseline case with a freestream velocity of 0.183 m/sec and a TSR value of 2.5 has been numerically simulated. Subsequently, various symmetric airfoils were analyzed under this frozen operating condition to discern their performance coefficients.

Figures 9c illustrates the tangential force coefficient on the blade surface of different symmetric blades of thickness ranging from 12 to 25 percent studied at a TSR of 2.5. The airfoil profile with a thinner cross-section performs better (with a higher torque coefficient) at the specified tip speed ratio over the entire rotation, even though the difference between the results of the NACA blades is small. It can be observed that

the thinner blade experiences a larger pressure difference between the upper and lower sides of the blade. For the same geometric angle of attack, the thinner blade generates a higher lift force. This result agrees with the study performed by [30] but contradicts the analysis of [34] who computed the flow for a wide range of turbine Reynolds numbers and tip speed ratios. However, [34] used a multiple-streamtube model and also depended on static airfoil data that showed thicker airfoils to outperform the thinner ones.

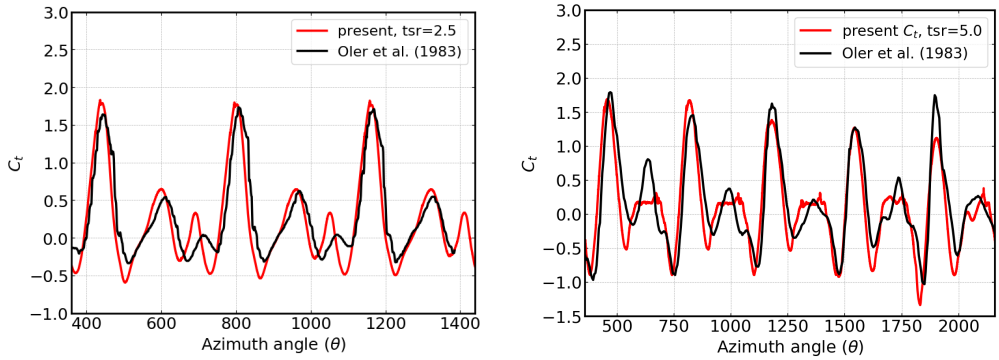

Figure 10: Comparison of tangential force coefficient of SM with the experiments of Oler et. al., [24], (a) $tsr = 2.5$, and (b) $tsr = 5.0$.

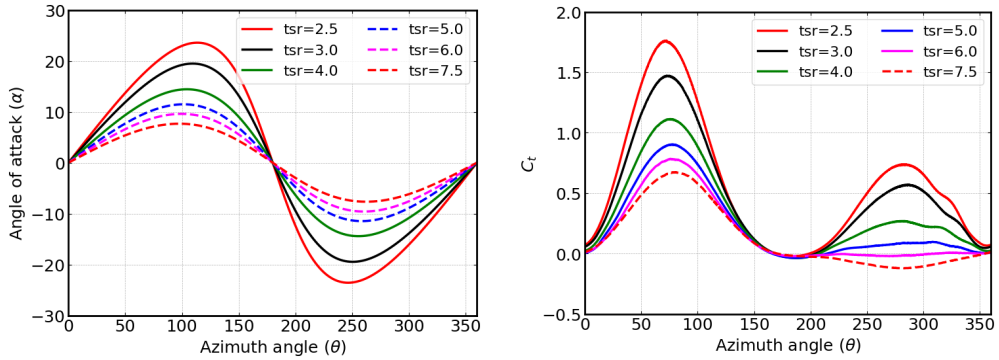

Figure 11: (a) Flow incidence angle (α) versus the blade azimuth position for different tip speed ratios λ, (b) variation of tangential force coefficient versus the blade position for different tip speed ratios λ.

In the upwind pass of Figures 10a, the power extracted is very high while in the downwind pass the speed is highly reduced and the simulated tangential, and normal forces are very low. The simulation is in good agreement with the general pattern of the experimental data. However, the simulation show over prediction at around $\theta = 90°$ and under predicted at around $\theta = 270°$. Even though our simulation conditions are identical, the meshing strategy used is different. One reason for the small discrepancy may be because [24] used a low aspect ratio blade for his experiment that might indicate

the presence of 3D effect. Another reason, for the over-predicted simulation is due to the consideration of low Reynolds number which decreases the lift and increases the drag of the blade, [1, 35].

Figures 11 presents the simulation for different tip speed ratios (λ). Figures 11a shows the flow incidence angle (α) versus azimuth position (θ) of the blade for different λ. Figures 11b depicts the variation of C_t for different tip speed ratios (λ).

The overset mesh technique is initially evaluated using different Reynolds numbers to ascertain its accuracy and efficiency. This evaluation entails investigating different flow configurations and complexities with the objective to validate the capability of overset meshes in accurately simulating flows with low to intermediate Reynolds numbers.

Figure 12, depicts the coefficient of lift for a flapping airfoil subjected to heaving and pitching motions at Reynolds number $Re = 1000$. The results demonstrate satisfactory agreement with the reference data [36], effectively capturing the essential features of the lift curve. Additionally, Figure 13 presents the lift coefficient for a pure plunging airfoil at a slightly higher Reynolds number, $Re = 4 \times 10^4$, showing good agreement with the reference data [37].

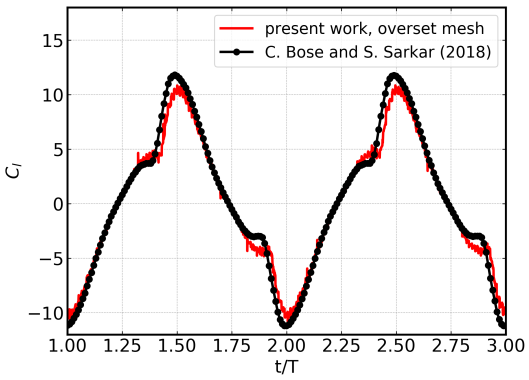

Figure 12: Pitching-plunging airfoil at $Re = 1000$, comparison of the lift coefficient C_l with [36] in the third revolution.

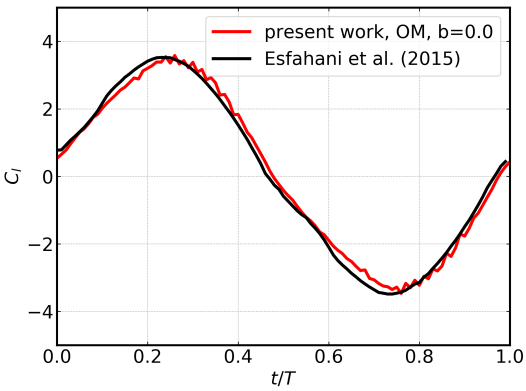

Figure 13: Pure-plunging airfoil at $Re = 4 \times 10^4$, comparison of the lift coefficient C_l with [37] in the fifth cycle.

Figure 14 compares the simulated results of a single-blade VAT based on the sliding and the overset meshes [19]. Both approaches predict the tangential force coefficient very well with the overset mesh showing minor discrepancies, however, all major features of the curve match satisfactorily. The capability of the overset mesh method to utilize `tabulated6DoF` Motion makes it more convenient for simulating more complex motions.

While the sliding mesh is a typical modeling technique for wind and hydrokinetic turbines, the overset method is also rarely used for such applications. However, there is little or no standard guideline for the design, simulations, and analysis of such systems using CFD in the literature and the available best practices differ from one to the other. The current work presents the methodology for accurate simulation of a VAT employing the above approaches. Single to multiple-bladed turbines can now be analyzed using

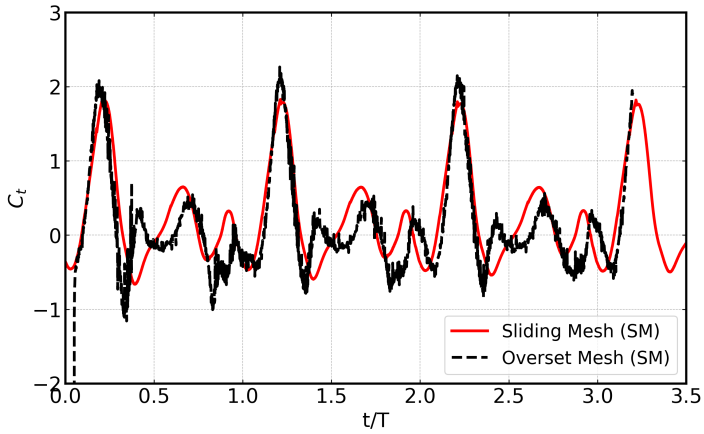

Figure 14: Comparison of the tangential force coefficient of VAT simulation based on sliding and overset meshes, over three cycles.

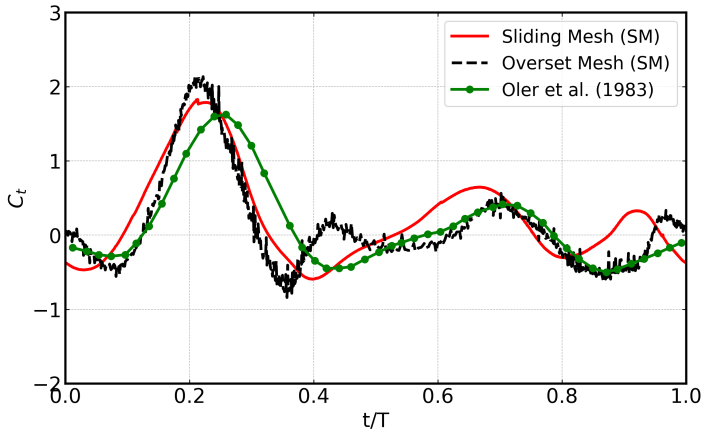

Figure 15: Comparison of the tangential force coefficients of sliding mesh, overset meshes, with experiment over one cycles.

OpenFOAM CFD with a lesser number of cells. For a single-blade simulation, the SM and OM predicted all the major features of the torque curve very well and with almost similar accuracy. The comparison of these dynamic mesh techniques by [14] reported that the peak of the torque curve is predicted at different TSRs and that the OM method converges faster.

4.2. Flow Field Simulation

Figure 16 shows snapshots of the vorticity distribution and the associated mesh during two periods of turbine revolution at four different time steps. The vorticity distribution shows a similar pattern for the sliding mesh and overset mesh cases. The left row indicates the mesh motion. The snapshots in the middle and right rows indicate the results obtained using the sliding and overset meshes, respectively.

Figure 2, the optimal performance for a VAT occurs when the blade aligns near the perpendicular position (90°) to the incoming flow in the upwind, as confirmed by [38, 39]. The flow velocity is optimal at that position where the blade sees an effective angle. The track of the turbine blade can be described in four segments: `windward`, `upwind`, `leeward`, and `downwind`. Different aerodynamic feature occurs in each segment. As depicted in Figure 15, the torque profile is least favorable in the leeward segment, where the airfoil aligns with the flow direction. Similarly, the downwind side of the windward segment exhibits notably low torque. Further exploration into the aerodynamics of the blade on an altered trajectory is provided in subsequent sections.

Figure 16 is a qualitative visualization of the vorticity field when the blade is at different positions of the curved and straight line paths during its motion. The blade aerodynamics is more complex around the leeward segment, and the observed behavior can be discussed as:

`Leeward` segment: The incoming flow velocity exceeds the blade velocity in this region (for the simulated TSR of 2.5), leading to a stronger interaction between the blades and the wake. This generates vorticity due to flow separation and mixing.

Lower left end: As the blade reverses its direction and enters the leeward segment, it encounters the previously shed vortices. This sudden change in direction combined with the existing wake leads to significant flow separation and vorticity production in this region.

Lower right end: The shed vortices from previous cycles reach the lower right end before the blades arrive. This interaction between the faster-moving vortices and the incoming flow creates additional vorticity and complex flow patterns.

5. Strengths and Limitations

5.1. Sliding mesh technique:

The sliding mesh method involves moving or deforming the mesh to accommodate the motion of the domain. The mesh is updated at each time step based on the motion of the domain. It has been extensively studied and improved over the years, and its strengths and weaknesses are well known.

The Sliding mesh has limitations in that it only supports a single form of mesh motion or a single topological change within a simulation. This limitation arises because SM depends on the dynamic mesh functionality of the AMI technique, which also requires the geometry to be a symmetrical kind. However, this weakness is replaced in OpenFOAM version 10 which the developers have redesigned it using the non-conformal coupling (NCC) technique [40].

Strengths:

- The sliding mesh is computationally efficient since the mesh is updated locally around the moving objects, rather than globally over the entire domain. This can significantly reduce computational costs and enable faster simulations.
- The sliding mesh technique is suitable to model the rotation of wind turbines. Recent studies show that it can be applied for moving cases with multi-degree-of-freedom such as the combined motions of an underwater vehicles.

Weaknesses:

- SM can lead to mesh distortion, which can affect the accuracy and stability of the simulation.
- SM can be challenging to implement for complex geometries or complex motions.
- SM can result in poor-quality mesh elements, especially near moving objects, which can affect the accuracy of the simulation.

5.2. Overset mesh technique:

The overset mesh method works by creating separate meshes for the moving and stationary domains for the convenience of operating motion functions. A composite mesh is created by patching together the individual meshes using the `mergeMeshes` utility. The overset grid approach offers the convenience of mesh generation and the capability to produce comparable results for complex systems without the drawbacks of mesh deformation. This approach combined with its flexibility proves valuable in exploring ingenious configurations that aim to improve the aerodynamic efficiency of Vertical Axis Turbines. A few examples of clever turbine designs include the dual-axis VAT proposed by [41], the variable geometry oval trajectory VAT concept introduced by [42], and investigations involving variable pitch scenarios as documented in [13]. Moreover, when combined with dynamic mesh techniques like mesh morphing, it becomes possible to shape the blade in specific regions for enhanced performance. The overset mesh technique has undergone substantial research and development, and both its advantages and disadvantages have been well known.

Strengths:

- Overset meshes can handle complex motions and geometries efficiently and excels very well, the SM technique struggles in such cases. Examples are, two cylinders moving toward each other with large relative displacements, track-based vertical axis turbine motion, and flapping of airfoils around an elliptic trajectory.
- It has proven capability of handling multi-body motions, such as the flapping of multiple wings, or the motion of multiple vehicles moving in close proximity to one another.
- It maintains the mesh quality close to moving objects which enhances simulation stability and accuracy. It outperforms the sliding mesh technique for such cases.
- It can be used for modeling multiple moving objects with diverse motions, which is hard to do using the sliding mesh approach and other capabilities in OpenFOAM.

Weaknesses:

- The interpolation methods for overset are not mas conservative [43]. To minimize the error, the background and the overset meshes should have similar cell sizes near the interface. It can also add numerical diffusion to the solution.
- Can be computationally expensive. When multiple moving meshes are used, all need to be patched together and this can slow the simulation by unpredictable factor.
- Rare discontinuities at the interface between moving and stationary geometries.

6. Conclusions

An appropriate meshing technique for Vertical Axis Turbine (VAT) simulations is crucial due to the complex flow field surrounding the moving blades. This study evaluated the performance of two common methods: Sliding Mesh (SM) and Overset Mesh (OM). Both approaches were applied to a baseline VAT case and validated against established benchmarks.

The findings suggest that sliding mesh approach offers a computationally efficient solution for VAT simulations with simple geometries and rigid body motions. It's particularly suited for baseline VAT analysis, especially at higher speed ratios. However, its limitations in handling complex motions and blade modifications restrict its applicability for innovative designs.

Overset mesh excels at simulating VATs with complex kinematics, including morphing blades and localized modifications. This enables targeted performance optimization in specific turbine regions. Additionally, OM maintains good mesh quality near moving objects, a crucial advantage for complex scenarios. While potential drawbacks include non-conservative interpolation methods and increased computational cost, the flexibility and accuracy of OM make it a valuable tool for analyzing advanced VAT designs.

Acknowledgments

We thank the Aerospace Computational Engine (ACE) at the Department of Aerospace Engineering, Indian Institute of Technology Bombay for providing computational resources. Additionally, we thank the organizing committee of the 18th OpenFOAM Workshop for their invaluable support. The first author acknowledges with gratitude the support received from (1) the Indian Institute of Technology Bombay, (2) Wolf Dynamics OpenFOAM training, (3) sponsors of the 18th OpenFOAM Workshop, and (4) organizers of the 18th OpenFOAM Workshop, all of which significantly contributed to the success of this work.

References

[1] Hansen J T, Mahak M and Tzanakis I 2021 *Renewable Energy* **171** 1371–1381
[2] Bianchini A, Balduzzi F, Bachant P, Ferrara G and Ferrari L 2017 *Energy Conversion and Management* **136** 318–328
[3] McCollum D, Gomez Echeverri L, Riahi K and Parkinson S 2017
[4] Sane S, Sudhakar K, Fernandes B and More D 2006 *Advances in Energy Research*
[5] Dabiri J O 2011 *Journal of renewable and sustainable energy* **3** 043104
[6] Ghasemian M, Ashrafi Z N and Sedaghat A 2017 *Energy Conversion and Management* **149** 87–100
[7] Hand B, Kelly G and Cashman A 2021 *Renewable and Sustainable Energy Reviews* **139** 110699
[8] Zhao Z, Wang D, Wang T, Shen W, Liu H and Chen M 2022 *Sustainable Energy Technologies and Assessments* **49** 101789
[9] Bhutta M M A, Hayat N, Farooq A U, Ali Z, Jamil S R and Hussain Z 2012 *Renewable and Sustainable Energy Reviews* **16** 1926–1939
[10] Kumar R, Raahemifar K and Fung A S 2018 *Renewable and Sustainable Energy Reviews* **89** 281–291
[11] Karmakar S D and Chattopadhyay H 2022 *Sustainable Energy Technologies and Assessments* **53** 102469
[12] Balduzzi F, Bianchini A, Maleci R, Ferrara G and Ferrari L 2016 *Renewable Energy* **85** 419–435
[13] Minetto R A L and Paraschivoiu M 2020 *Energy* **202** 117705
[14] Lopez Mejia O D, Mejia O E, Escorcia K M, Suarez F and Laín S 2021 *Processes* **9** 1933
[15] Baghdadi M, Elkoush S, Akle B and Elkhoury M 2020 *Renewable Energy* **154** 239–251

[16] Weller H G, Tabor G, Jasak H and Fureby C 1998 *Computers in physics* **12** 620–631
[17] Windt C, Davidson J and Ringwood J V 2018 *Renewable and Sustainable Energy Reviews* **93** 610–630
[18] Fertahi S e D, Belhadad T, Kanna A, Samaouali A, Kadiri I and Benini E 2023 *Fluids* **8** 242
[19] Guerrero J 2006 *DICAT, University of Genoa, Italy*
[20] Holzmann T 2017 Mathematics, numerics, derivations and openfoam (r), holzmann cfd
[21] Ferziger J H and Perić M 2002 *Computational methods for fluid dynamics* vol 3 (Springer)
[22] Maric T, Höpken J and Mooney K The openfoam technology primer (sourceflux, duisburg, 2014)
[23] Jasak H and Tuković Ž 2010 *Proceedings of the V European Conference on Computational Fluid Dynamics ECCOMAS CFD 2010*
[24] Oler J, Strickland J H, Im B and Graham G 1983 Dynamic-stall regulation of the darrieus turbine Tech. rep. Texas Tech Univ., Lubbock (USA). Dept. of Mechanical Engineering
[25] Inc O Onshape: 3d cad software for everyone online software URL https://www.onshape.com/
[26] Aqilah F, Islam M, Juretic F, Guerrero J, Wood D and Ani F N 2018 *IIUM Engineering Journal* **19** 203–212
[27] Laws P, Saini J S and Kumar A 2019
[28] Nordanger K, Holdahl R, Kvarving A M, Rasheed A and Kvamsdal T 2015 *Computer Methods in Applied Mechanics and Engineering* **284** 664–688 ISSN 0045-7825 isogeometric Analysis Special Issue URL https://www.sciencedirect.com/science/article/pii/S0045782514004034
[29] Rogowski K 2019 *Energies* **12** 2506
[30] Danao L A, Qin N and Howell R 2012 *Proceedings of the Institution of Mechanical Engineers, Part A: J. of Power and Energy* **226** 867–881
[31] Patankar S V and Spalding D B 1983 *A calculation procedure for heat, mass and momentum transfer in three-dimensional parabolic flows* (Pergamon: Elsevier)
[32] Hansen M 2008 *Sterling, VA*
[33] Durrani N, Hameed H, Rahman H and Chaudhry S 2011 *49th AIAA aerospace sciences meeting including the new horizons forum and aerospace exposition* p 541
[34] Healy J 1978 *Wind Engineering* 1–9
[35] Chong W, Fazlizan A, Poh S, Pan K, Hew W and Hsiao F 2013 *Applied Energy* **112** 601–609
[36] Bose C, Gupta S and Sarkar S 2021 *Journal of Fluid Mechanics* **911** A31
[37] Esfahani J, Barati E and Karbasian H R 2015 *Computers & Fluids* **108** 142–155
[38] Porté-Agel F, Bastankhah M and Shamsoddin S 2020 *Boundary-Layer Meteorology* **174** 1–59
[39] Paraschivoiu I, Ammar S and Saeed F 2018 *Transactions of the Canadian Society for Mechanical Engineering* **42** 393–403
[40] Greenshields C and Weller H 2022 *Notes on Computational Fluid Dynamics: General Principles* (Reading, UK: CFD Direct Ltd)
[41] Naccache G and Paraschivoiu M 2017 *J. of Fluids Engineering* **139**
[42] Ponta F, Seminara J and Otero A 2007 *Renewable energy* **32** 35–56
[43] Alletto M 2022 *OpenFOAM® Journal* **2** 13–30

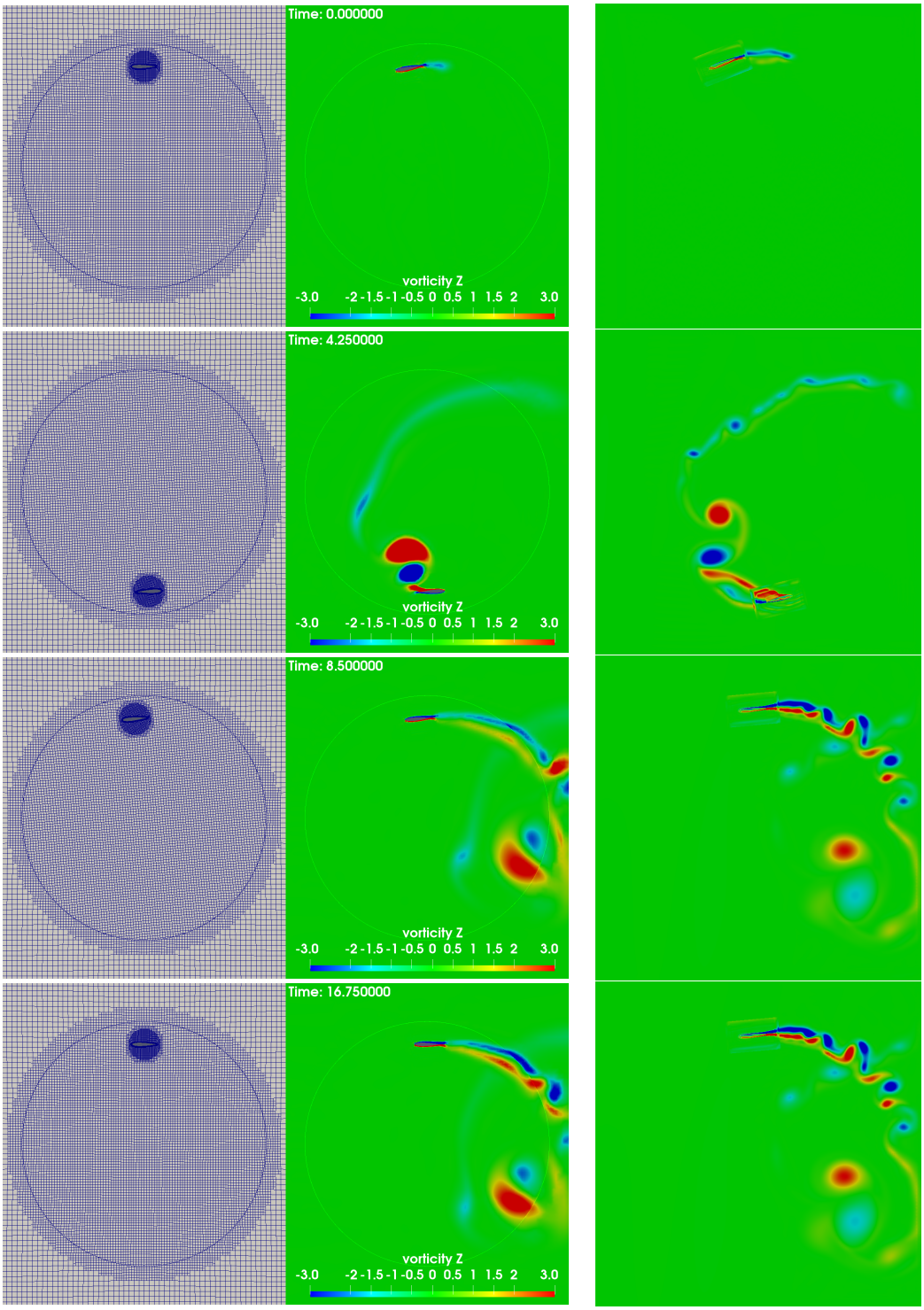

Figure 16: VAT simulation based on sliding and overset meshes, mesh visualization (left) and vorticity distribution over two complete cycles; SM (middle) and OM (right).